

MIT Open Access Articles

The Dynamic Compressive Response of an Open-Cell Foam Impregnated With a Non-Newtonian Fluid

The MIT Faculty has made this article openly available. **Please share** how this access benefits you. Your story matters.

Citation: Dawson, M. A., G. H. McKinley, and L. J. Gibson. "The Dynamic Compressive Response of an Open-Cell Foam Impregnated With a Non-Newtonian Fluid." *Journal of Applied Mechanics* 76 (2009): 061011. ©2009 American Society of Mechanical Engineers.

As Published: <http://dx.doi.org/10.1115/1.3130825>

Publisher: American Society of Mechanical Engineers

Persistent URL: <http://hdl.handle.net/1721.1/67019>

Version: Final published version: final published article, as it appeared in a journal, conference proceedings, or other formally published context

Terms of Use: Article is made available in accordance with the publisher's policy and may be subject to US copyright law. Please refer to the publisher's site for terms of use.



The Dynamic Compressive Response of an Open-Cell Foam Impregnated With a Non-Newtonian Fluid

M. A. Dawson

G. H. McKinley

Department of Mechanical Engineering,
Massachusetts Institute of Technology,
Cambridge, MA 02139

L. J. Gibson

Department of Materials Science and
Engineering,
Massachusetts Institute of Technology,
Cambridge, MA 02139

The response of a reticulated, elastomeric foam filled with colloidal silica under dynamic compression is studied. Under compression beyond local strain rates on the order of 1 s^{-1} , the non-Newtonian, colloidal silica-based fluid undergoes dramatic shear thickening and then proceeds to shear thinning. In this regime, the viscosity of the fluid is large enough that the contribution of the foam and the fluid-structure interaction to the stress response of the fluid-filled foam can be neglected. An analytically tractable lubrication model for the stress-strain response of a non-Newtonian fluid-filled, reticulated, elastomeric foam under dynamic compression between two parallel plates at varying instantaneous strain rates is developed. The resulting lubrication model is applicable when the dimension of the foam in the direction of fluid flow (radial) is much greater than that in the direction of loading (axial). The model is found to describe experimental data well for a range of radius to height ratios ($\sim 1\text{--}4$) and instantaneous strain rates of the foam (1 s^{-1} to $4 \times 10^2\text{ s}^{-1}$). The applicability of this model is discussed and the range of instantaneous strain rates of the foam over which it is valid is presented. Furthermore, the utility of this model is discussed with respect to the design and development of energy absorption and blast wave protection equipment. [DOI: 10.1115/1.3130825]

Keywords: foam, lubrication approximation, non-Newtonian, porous media, shear-thickening fluid

1 Introduction

While existing armor is highly advanced and capable of resisting most projectiles [1], advancements toward the development of an armor that efficiently protects against the enormous pressure gradients generated by explosive devices are limited. Blast waves can cause severe damage to the human body as well as to vehicles and structures. Recently, the design of a novel reactive armor to mitigate the effects of blast waves has been explored [2]. This design incorporates open-cell (reticulated) foams filled with shear-thickening, non-Newtonian liquids into existing composite armor. Open-cell foams filled with non-Newtonian liquids have the potential to impede shockwaves, increasing the time it takes for waves to propagate through the foam medium and decreasing the resulting pressure gradient experienced by underlying media (e.g., tissue). As a first step in modeling this nonlinear phenomenon, we analyze the flow of a non-Newtonian fluid (NNF), which has a shear-thickening regime, through an open-cell, elastomeric foam. The flow of both Newtonian and non-Newtonian fluids through open-cell foams has been investigated extensively for a variety of engineering applications, but characterizing the contribution of the fluid to energy absorption under dynamic loading is still a critical area of research. Most of the previous research has focused on the development of complex, often computational, models to describe the contribution of Newtonian fluids in an open-cell foam under impact loading [3–6]. More recent work by Dawson et al. [7] has resulted in the development of tractable models for the contribution of viscous Newtonian flow to the stress-strain response of a low-density, reticulated, fluid-filled foam under dynamic loading.

However, comparably little work has been done in the field of non-Newtonian flow through deformable porous media. While a number of authors have studied the pressure drop of general power-law, non-Newtonian fluids through porous media [8–10], a comparable model for the response of a non-Newtonian fluid-filled foam under dynamic compression has not been published.

In this paper, we analyze the response of a NNF-filled, low-density, reticulated, elastomeric foam under dynamic axial compression. The response after the fluid has undergone shear thickening is particularly important since the fluid will nearly always be in this regime for most engineering designs under dynamic loading. Scaling arguments demonstrate that after the shear-thickening transition, the contribution of the foam itself and the contribution of the fluid-structure interaction to the overall response can be neglected. Based on these arguments, a lubrication model for squeezing flow of a non-Newtonian fluid between two parallel plates is developed in which the characteristic dimension of the fluid in the direction of fluid flow (radial) is assumed to be much greater than that in the direction of loading (axial). The corresponding range of instantaneous strain rates of the NNF-filled foam over which this model is applicable is also given. It is anticipated that this model is applicable for nearly all expected instantaneous strain rates caused by either impact loading or blast wave loading. The range of characteristic dimensions of the NNF-filled foam over which this model is valid is also given based on previous research on the applicability of a lubrication model to the stress-strain response of a Newtonian fluid-filled foam under dynamic compression [7]. The lubrication model is analytically tractable, depending only on the characteristic fluid properties, the characteristic radius to height ratio of the NNF-filled foam, and the instantaneous strain rate of the foam. Furthermore, it is independent of all of the parameters of the low-density, elastomeric foam, such as foam grade.

Experimental measurements of the stress-strain response of a

Contributed by the Applied Mechanics Division of ASME for publication in the JOURNAL OF APPLIED MECHANICS. Manuscript received March 6, 2008; final manuscript received March 23, 2009; published online July 23, 2009. Review conducted by Nesreen Ghaddar.

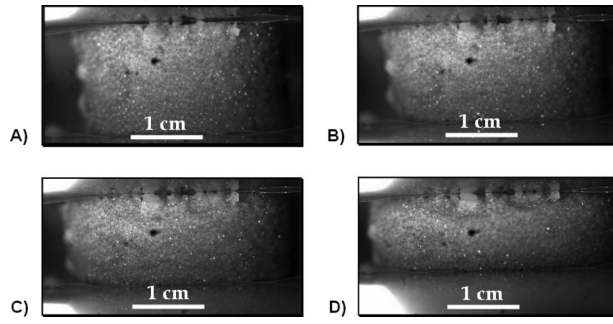


Fig. 1 Images of a 70 pores/in. foam filled with 61% volume fraction silica-based non-Newtonian fluid loaded in axial compression at 250 mm/s. (a) $\varepsilon=0$ strain, (b) $\varepsilon=0.1$ strain, (c) $\varepsilon=0.2$ strain, and (d) $\varepsilon=0.3$ strain.

low-density polyurethane foam filled with a colloidal silica non-Newtonian fluid under dynamic loading are presented. The non-Newtonian fluid is comprised of a high volume fraction of nearly monodisperse silica particles suspended in ethylene glycol. Shear thickening is often observed in concentrated colloidal dispersions and is characterized by a dramatic increase in viscosity with increasing shear stress in the fluid [11,12]. Numerous studies have concluded that reversible shear thickening in colloidal suspensions is due to the formation and jamming of clusters of particles (hydroclusters) bound together by hydrodynamic lubrication forces between particles [13–16]. Detailed reviews and quantitative descriptions of the mechanisms for shear thickening of colloidal suspensions are given in Refs. [17–19]. In this paper, the complex behavior of colloidal silica non-Newtonian fluid is discussed and related to the response of the NNF-filled foam. In the range where the model is valid, it is found to be strongly supported by experimental results. Finally, a brief discussion of the engineering applications of non-Newtonian fluid-filled foams and the significance of the model presented in this paper are presented.

2 Analysis

2.1 Model Assumptions. This analysis considers dynamic axial compression of a low-density, elastomeric foam fully saturated with a non-Newtonian power-law fluid between two parallel plates. The fluid is assumed to remain in a cylindrical shape with uniform radius while undergoing deformation, where the radius of the cylinder can be determined by conservation of mass of an incompressible fluid (Fig. 1). In addition, the fluid is assumed to be a power-law fluid with a highly shear-thickening regime, such that the maximum viscosity is several orders of magnitude greater than the minimum viscosity. For known nanoparticle based non-Newtonian fluids, this will result in a maximum viscosity greater than 10^3 Pa s. In this viscosity range, the stress within the fluid is three orders of magnitude greater than that in the foam alone. Furthermore, the characteristic dimension of the colloidal particles in the fluid is several orders of magnitude smaller than the characteristic dimension of the foam pore size. These two observations ensure that the response of the elastomeric foam, as well as the fluid-structure interaction between the foam and the non-Newtonian fluid, can be neglected, so that the system behaves as if the foam were nonexistent. This assumption is supported in Fig. 2 where magnified images of the cells of the foam are shown before loading and during loading. In Fig. 2 it is evident that the foam struts are readily torn apart by the highly viscous fluid flow, supporting the hypothesis that the structural support from the foam and the fluid-structure interaction is negligible. This result is in contrast to the result presented by Dawson et al. [7] for a lower viscosity, Newtonian fluid-filled foam where the structural response of the foam and the fluid-structure interaction are significant. The analysis presented in this paper is also based on a lubri-

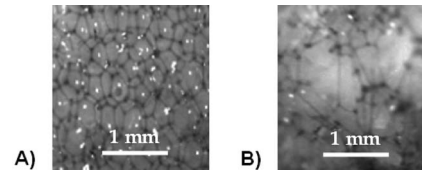


Fig. 2 Optical micrograph of a NNF-filled foam. (a) $\varepsilon=0$ strain and (b) $\varepsilon=0.4$ strain.

cation approximation, which assumes that the ratio of the characteristic radius of the specimen to the characteristic height of the specimen, in this paper referred to as the aspect ratio, is much greater than 1. Dawson et al. [7] gave a detailed analytical description of the applicability of the lubrication approximation to a comparable problem with a Newtonian fluid and demonstrated the rapid convergence of the lubrication model to the exact solution as the aspect ratio increases. They concluded that beyond aspect ratios of 4, the lubrication model can be used to approximate the exact solution; however, even beyond aspect ratios of unity, the lubrication solution is shown to approximate the exact solution to within 10% for most strains. Finally, after the shear-thickening transition, the flow is assumed to be dominated by viscous forces for all instantaneous strain rates of the foam considered in this analysis.

2.2 Fluid Flow in a Rectangular Channel. We first consider a model for pressure driven flow of a power-law fluid through a rectangular channel (Fig. 3) where the length of the channel is L , the width is W , and the height is $2B$ with $2B \ll W \ll L$. The flow is assumed to be incompressible and locally fully developed. The gravitational effects are assumed to be negligible. Since the flow is assumed to be dominated by viscous forces, inertial effects can also be neglected. The following velocity and pressure profiles are assumed:

$$\begin{aligned} V_z &= V_z(x, y) \\ V_x &= V_y = 0 \\ P &= P(z) \end{aligned} \quad (1)$$

where V_x , V_y , and V_z are the velocity components in the horizontal (x), vertical (y), and axial (z) directions, respectively, and P is the local pressure within the fluid. Coupling the equation of continuity with the full Navier–Stokes equations of motion, this problem is readily solved for a power-law fluid where the viscosity η is given by the relation

$$\eta = m(\dot{\gamma})^{n-1} \quad (2)$$

where m is the consistency index, n is the power-law exponent, and $\dot{\gamma}$ is the magnitude of the rate of strain tensor or the shear rate of the fluid. Following Bird et al. [20], the necessary boundary conditions are based on symmetry and no wall-slip at the wall and can be given by

$$\begin{aligned} \tau_{yz}|_{y=B} &= 0 \\ V_z|_{y=0} &= 0 \end{aligned} \quad (3)$$

where τ_{yz} is the shear stress in the fluid. Applying these assumptions and boundary conditions, the Navier–Stokes equations of

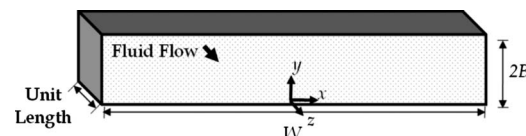


Fig. 3 Model of rectangular channel flow

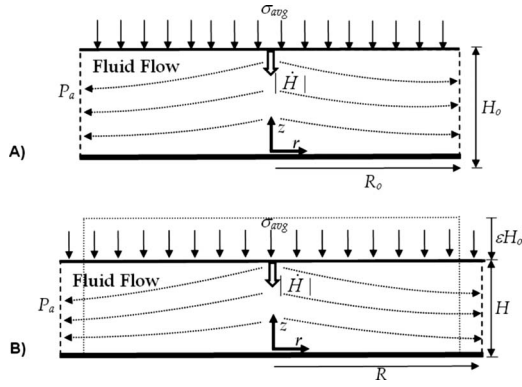


Fig. 4 Lubrication fluid flow model assuming the absence of foam. (a) At 0 strain and (b) at any given strain ϵ .

motion in the axial direction can be solved using a lubrication approximation. The resulting flow rate Q , given by Bird et al. [20], is found to be

$$Q = 2WB^2 \left(-\frac{B}{m} \frac{\partial P}{\partial z} \right)^{1/n} \frac{1}{\left(\frac{1}{n} + 2 \right)} \quad (4)$$

2.3 Radial Fluid Flow in a Cylindrical Specimen Squeezed Between Parallel Plates. In the lubrication limit, flow in a rectangular channel can be transformed to radial squeezing flow between two parallel plates where the lower plate is fixed and the upper plate is moving as shown in Fig. 4. As previously discussed, the fluid is assumed to remain in a cylindrical shape with uniform radius while undergoing deformation. By conservation of mass the aspect ratio at any given axial strain ϵ is given by

$$\frac{R}{H} = \frac{R_o}{H_o} \left[\frac{1}{1 - \epsilon} \right]^{3/2} \quad (5)$$

where R_o is the initial radius of the NNF-filled foam at zero strain, H_o is the initial height at zero strain, R is the radius at any given strain, H is the distance between the plates, and ϵ is the strain, taken to be positive in compression and given by $(1 - H/H_o)$ (Fig. 4). In Fig. 4 P_a is the atmospheric pressure on the free surface, and the magnitude of the velocity of the top plate is given by $|\dot{H}|$, where \dot{H} is the time rate of change in the distance between the two plates. Using the transformations from the two-dimensional, rectangular channel, planar flow problem in Sec. 2.2 to the squeezing flow problem between parallel plates in cylindrical coordinates given by Bird et al. [20], Eq. (4) can be rewritten for the lubrication squeezing flow between parallel plates as

$$Q(r) = \pi r H^2 \left(-\frac{H}{2m} \frac{\partial P}{\partial r} \right)^{1/n} \frac{1}{\left(\frac{1}{n} + 2 \right)} \quad (6)$$

Furthermore, the equation of continuity can be used to find a relation between the volumetric flow rate and the change in height of the fluid giving

$$Q(r) = \pi r^2 (-\dot{H}) \quad (7)$$

Combining Eqs. (6) and (7) and solving for the pressure profile give

$$P(r) - P_a = \frac{2m(-\dot{H})^n}{H^{2n+1}} \left(\frac{2n+1}{n} \right)^n \frac{R^{n+1}}{n+1} \left[1 - \left(\frac{r}{R} \right)^{n+1} \right] \quad (8)$$

For a power-law fluid σ_{zz} is zero on the surface of the plate by arguments of the equations of motion in the normal direction and mass conservation under a no slip condition. Furthermore, Bird et

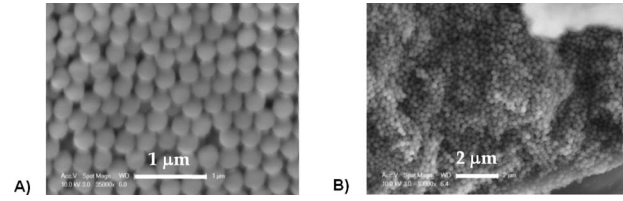


Fig. 5 Scanning electron microscope images of silica particles

al. [20] gave the solution for squeezing flow of viscoelastic fluids between parallel disks, accounting for normal stresses using the Criminale-Ericksen-Filbey (CEF) equations. It is evident that the pressure distribution given in Eq. (8) is equivalent to this solution, indicating normal stress effects σ_{zz} on the surface of the plate are negligible. Neglecting inertial effects, a force balance can be used to find an equivalent uniform stress distribution or true stress σ_{avg} , applied to the top compression plate by integrating the pressure field over the radius and dividing by the area of the plate giving

$$\sigma_{avg} = 2 \left(\frac{2n+1}{n} \right)^n \frac{m}{n+3} \left(\frac{R_o}{H_o} \right)^{n+1} \left(\frac{-\dot{H}}{H} \right)^n \left(\frac{1}{1-\epsilon} \right)^{3(n+1)/2} \quad (9)$$

where $-\dot{H}/H$ is the instantaneous strain rate of the NNF-filled foam or the negative of the current rate of change in the height of the foam divided by the current height of the foam. It is important to distinguish the instantaneous strain rate of the foam from the magnitude of the strain rate of the fluid $\dot{\gamma}$, which in this paper is referred to as the local strain rate. In our experiments described below, the fluid flows through an open-cell foam, which introduces a tortuosity to the fluid path. We account for the tortuosity by introducing a constant into Eq. (9).

3 Experimental Methods

3.1 Materials. Specimens of open-cell, flexible, polyester-based polyurethane foams (New Dimension Industries, Moonachie, NJ), with nominal cell diameters of 175 μm , 210 μm , and 235 μm (corresponding to manufacturer specified grades of 90 pores/in., 80 pores/in., and 70 pores/in., respectively) were used in the experiments. The densities of the foams ranged from 0.0318 g/cm^3 to 0.0322 g/cm^3 . Based on the manufacturer's value of the density of the solid polyurethane ($\rho_s = 1.078 \text{ g}/\text{cm}^3$), the relative density of the foams was $\rho_o^*/\rho_s \approx 0.030$. The foam was cut into cylindrical specimens with nominal diameter $D = 25.4 \text{ mm}$ and height $H_o = 12.6 \text{ mm}$. The dimensions of each sample were measured using a digital caliper accurate to within 0.01 mm.

The non-Newtonian fluid consisted of silica nanoparticles (Fuso Chemical Co., Osaka, Japan) suspended in ethylene glycol (VWR, West Chester, PA) at a volume fraction of approximately 61%. The average particle diameter was determined using a scanning electron microscope (XL30 FEG ESEM, FEI/Philips, Hillsboro, OR) as shown in Fig. 5(a). The diameters of 100 particles were measured and analyzed using SCION IMAGE analysis software (Scion Corporation, Frederick, MD). The particles are found to be nearly monodisperse (Fig. 5(b)) with an average diameter of 293 $\text{nm} \pm 31 \text{ nm}$. The density of the silica nanoparticles themselves was taken to be that given by the supplier of 1.95 g/cm^3 . The density and viscosity of the ethylene glycol suspending fluid were taken to be $\rho = 1.11 \text{ g}/\text{cm}^3$ and $\mu = 2.1 \times 10^{-2} \text{ Pa s}$ at 20°C.

The colloidal silica suspension was first washed with ethylene glycol three times. The washing process began by centrifuging the solution at 2700 g for 4 h using a Sorvall Legend Mach 1.6 Centrifuge (Fisher Scientific, Suwanee, GA). After this centrifuging process, the silica suspension consisted of a sedimented layer and a layer of supernatant, which was subsequently poured off. Ethyl-

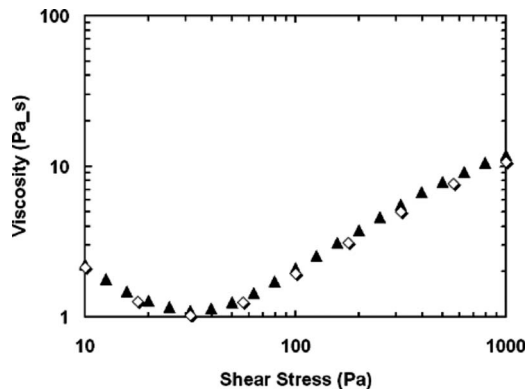


Fig. 6 Steady shear viscosity plotted against shear stress for 48% volume fraction of silica-based non-Newtonian fluid. Gap thickness: 500 μm (\blacktriangle) and 250 μm (\diamond).

ene glycol was then added to the remaining sedimented layer and the mixture was resuspended using a VWR digital vortex mixer (VWR, West Chester, PA). In order to determine the volume fraction of the sedimented silica particles after centrifuging and removal of the supernatant, the sediment was dried until no significant change in mass over a 24 h period was detected. Based on this drying experiment, the volume fraction of the sediment was determined to be 69% silica particles by volume. The volume fraction of the sediment after centrifuging and removal of the supernatant was found to be constant to within measures of uncertainty. In the experiments utilized for this paper the sediment was immediately redispersed in ethylene glycol after centrifuging to give a final suspension volume fraction of approximately 61% silica. To redisperse the sediment and create this 61% by volume silica-based NNF, a vortex mixer was used until the sediment appeared to be completely suspended in the fluid. Then the NNF was sonicated for 1 h using an ultrasonic bath. Based on the assumption of ideal mixing, the density of the resulting NNF was estimated to be 1.6 g/cm^3 .

3.2 Viscosity of the Silica Suspension. The steady state rheological properties of the colloidal silica suspension or non-Newtonian fluid under shear flow were then measured using a controlled stress rheometer (ARG 2000, TA Instruments, New Castle, DE). The geometry was selected to be a 40 mm aluminum parallel plate geometry with 500 μm gap. Although a cone and plate geometry is preferred for steady state shear properties, the parallel plate geometry is more suitable for use with sandpaper, which is required to reduce slip of a high viscosity fluid. A detailed discussion on the effects of wall slip in rheological measurements can be found in Ref. [21]. In summary, the presence of slip in viscosity measurements is detected by substantial shifts in the viscosity plots with varying gap thickness between the parallel plates (in some cases shifts in the viscosity can be in excess of an order of magnitude). To eliminate slip in the rheological measurements, the parallel plate geometry was covered with a 1000 grit sandpaper, for which the characteristic size of the grit or roughness is of the same order of magnitude as the diameter of the silica particles. The rheological measurements were found to be very similar with gap ranges varying from 250 μm to 1000 μm , indicating that this sandpaper nearly eliminated the effect of wall slip. Figure 6 gives a plot of the viscosity against the shear stress in the silica-based NNF with a volume fraction of approximately 48% measured at gaps of 250 μm and 500 μm . Figure 6 clearly demonstrates in these experiments that there was a negligible change in the viscosity with varying gap thickness, indicating slip was successfully eliminated. All experiments were performed at 22.5°C and controlled with a Peltier temperature control. After loading the sample into the viscometer, the sample was loaded under a preshear stress ramp from 10 Pa to 100 Pa and then

allowed to rest for 15 min to eliminate any effects of sample loading. A stress sweep was performed from 10 Pa to a maximum shear stress in the fluid of approximately 15,400 Pa with 10 points/decade, each of which was measured for 60 s. However, for samples with a lower volume fraction of particles than the standard 61% sample, the maximum shear stress value in the fluid could not be achieved due to rate limitations of the rheometer, so the maximum shear stress achievable was recorded. Ascending and descending stress sweeps were performed, and minimal hysteresis was observed, demonstrating the reversibility of the fluid as found by Bender and Wagner [17]. In addition, no yield stress behavior was observed at low stresses. The steady state shear viscosity was measured along with the shear stress in the fluid and local shear rate under controlled stress loading. Because of the complexity of the manufacturing process, determining the exact volume fraction of silica particles is difficult, so small variations in the volume fraction are expected. To assess the sensitivity to variations in the volume fraction of silica and to determine the overall characteristic behavior of high volume fraction silica-based fluids, this procedure was used for a range of volume fractions from 48% to 61%.

3.3 Dynamic Compression Tests on Non-Newtonian Fluid-Filled Foam. Samples of a reticulated, polyurethane foam saturated with the 61% volume fraction silica-based NNF were then prepared. Since even the minimum viscosity of the NNF is large, samples of a reticulated foam were filled by the capillary effect through compression cycles while submerged in a bath of NNF shaken by a vortex mixer. Hager and Craig [22] demonstrated that the deflection of a polyurethane foam compressed to 0.75 strain for a short duration of time is almost completely recoverable. Therefore, an attempt was made not to exceed a strain of 0.75 during the filling process to minimize the microstructural damage caused by the filling process. This filling procedure was carried out until the weight of the fluid-filled foam samples achieved the desired saturated weight expected, based on the density, porosity, and dimensions of the foam as well as the density of the fluid. After saturation, the NNF-filled foam was allowed to recover for 2 h prior to testing, based on data for the recovery of a low-density polyurethane foam presented by Hager and Craig [22].

The compressive true stress-strain response of the NNF-filled foam was measured with the rise direction of the foam parallel to the direction of loading, up to a strain of 0.6 strain and over a range of instantaneous strain rates of the foam from $-\dot{H}/H = 1.0 \text{ s}^{-1}$ to $4 \times 10^2 \text{ s}^{-1}$. For instantaneous strain rates less than $-\dot{H}/H = 50 \text{ s}^{-1}$ an Instron testing machine (Instron Model 1321, Instron Corp., Canton, MA) was used at constant velocities ($-\dot{H} = 12.5 \text{ mm/s}$, 31.25 mm/s, 62.5 mm/s, 93.75 mm/s, 125 mm/s, and 250 mm/s); for instantaneous strain rates greater than $-\dot{H}/H = 50 \text{ s}^{-1}$ a Dynatup drop-tower (Dynatup 9200 Series, Instron Corp., Canton, MA) was used. The drop-tower impact experiments were arranged to be nearly constant velocity. Data were only collected up to strains of approximately 50%, at which point built in stoppers in the drop tower absorbed the remaining energy. The drop-tower weight was approximately 21.7 kg, resulting in an impact energy that was substantially greater than the energy absorbed by the NNF-filled foam or the energy gained due to potential energy effects. Since the energy of the drop-tower weight was nearly constant, the resulting experiments were nearly constant velocity ($-\dot{H} \approx 0.75 \text{ m/s}$, 1.00 m/s, 1.25 m/s, 1.50 m/s, 1.75 m/s, 2.00 m/s, 2.25 m/s, 2.50 m/s, 2.75 m/s, and 3.00 m/s). During testing the temperature was maintained at 22.5°C to ensure the fluid properties are consistent. Since the flow is assumed to be instantaneously fully developed, the model presented in this paper is applicable to constant velocity loading.

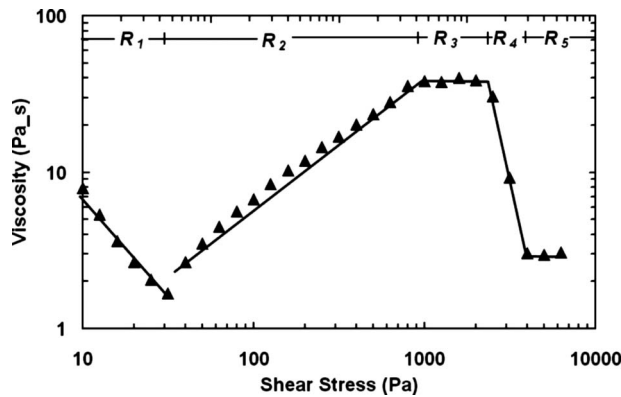


Fig. 7 Steady shear viscosity plotted against shear stress for 50% volume fraction silica-based non-Newtonian fluid

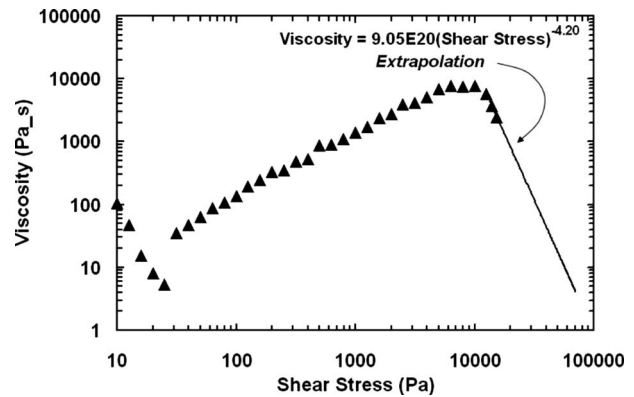


Fig. 8 Steady shear viscosity plotted against shear stress for 61% volume fraction silica-based non-Newtonian fluid

4 Fluid Viscosity Results and Discussion

In Fig. 7 a typical plot of the viscosity against the shear stress in the fluid for a NNF fluid with volume fraction of 50% silica particles is given. The rheological behavior of the fluid under steady state shear viscosity testing in the controlled stress rheometer was consistent for all volume fractions tested, so Fig. 7 is taken to be typical of the behavior for all silica-based, non-Newtonian fluids with the shear-thinning and -thickening regimes discussed in this paper. The viscosity data also correspond well with similar experiments performed by Maranzano and Wagner [18].

Figure 7 also denotes the typical regimes of distinct behavior observed for this class of fluids. At extremely low local strain rates the fluid acts as a shear-thinning fluid (regime R_1). The shear thinning or “yield stress” behavior observed at low shear stresses (or local strain rates) occurs when the particles in an ordered phase begin to orient themselves so that the direction of closest packing of the spheres aligns with the flow velocity, such that the planes containing the closest packing spheres are parallel to the shearing surfaces [23]. Therefore, the three-dimensional ordered phase transforms into a two-dimensional layered phase that permits flow, resulting in a dramatic drop in viscosity. At a critical shear stress (or local strain rate) dramatic shear thickening occurs, evident in regime R_2 . The onset of this dramatic shear thickening occurs when the hydrodynamic forces driving particles together exceed the repulsive forces due to interparticle (i.e., electrostatic or steric) potentials and Brownian motion [18], and the particles fail to remain in their ordered state and begin to form three-dimensional clusters of particles. This dramatic shear thickening is evident in Fig. 7 at nearly constant local strain rate. This dramatic shear thickening is often termed “critical shear thickening” as when a discontinuity is observed as shown in Fig. 7. As previously discussed the jamming phenomenon is attributed to shear thickening, but critical shear thickening is only observed for very high volume fractions of solid particles. Following shear thickening, a plateau viscosity is reached (regime R_3). A number of theories have been proposed for this phenomenon, but it is generally accepted that the clusters begin to break down and form a random three-dimensional packing [12]. These first three regimes are characteristic of most non-Newtonian fluids with shear-thickening regimes [12]. However, after the maximum plateau, the fluid is often found to enter one of three stages: fracture, an extended plateau viscosity independent of shear rate, or a shear-thinning regime [12]. This regime of behavior is controlled by particle size distribution, particle content, the volume fraction of particles, particle-particle interactions, and the viscosity of the continuous phase. For the particular fluid discussed in this paper, another shear-thinning regime, R_4 , occurs and, finally, for lower volume fraction fluids, a lower plateau viscosity is observed (regime R_5), which is approximately equal to the minimum viscosity previ-

ously obtained (Fig. 7). A large body of literature attempts to explain the behavior in all the regimes described [24,17,25,13] but the explanations for some phenomenon are still under dispute, so a detailed description is excluded from this paper. However, the general regimes described here are found to be consistent with this body of literature as seen in Refs. [26,12]. The primary remaining debate is around the shear-thinning regime R_4 and whether or not slip is causing it. In addition to the evidence presented by Hadjitsamov [26] and Barnes [12], Hoffman [11] also demonstrated distinct shear-thinning regimes after shear thickening for monodisperse polymeric resin colloids. We believe that much of the recent literature has avoided the debate around this topic by not publishing data in the high stress regime examined in this study. For instance, the maximum shear stresses examined for comparable silica-based non-Newtonian shear-thickening fluids given by Bender and Wagner [17], Fagan and Zukoski [27], Lee et al. [23], and Maranzano et al. [18] range from the order of 100 Pa to the order of 1000 Pa. None of these studies attempts to examine the stress regime approaching and exceeding 1×10^4 Pa, presented in this study. However, more recent studies by Egres and Wagner [28] demonstrated that measurements in this regime are possible. They also showed with a different type of shear-thickening fluid (precipitated calcium carbonate based shear-thickening-fluid (STF)) distinct plateau regimes, corresponding to R_3 , followed by, in some cases, what appears to be the beginning of shear-thinning regimes, corresponding to R_4 . In addition to this support, the results of the stress-strain response of the NNF-filled foam presented at the end of this paper provide further evidence that the apparent shear-thinning phenomenon in regime R_4 is not caused by slip.

Figure 8 plots the viscosity against the shear stress in the fluid for 61% volume fraction silica/ethylene glycol solution. Limitations in the maximum torque capacity of the viscometer did not allow us to obtain data for the full range of regimes R_4 and R_5 . Assuming that the trends in the viscosity of the fluid with 61% volume fraction silica particles are similar to those at lower volume fraction of particles, we can extrapolate the existing R_4 data using a linear regression of the log data (equations shown in the figures). We note that, for lower particle volume fraction based fluids, such as in Fig. 7, the value of the viscosity for the lower plateau (R_5) is similar to that at the minimum of R_1 ; we expect the transition from R_4 to R_5 to be similar for the fluid with 61% volume fraction of particles. In Fig. 8 an equation for the trend line of the viscosity as a function of the shear stress is given, which can be transformed into an equation for the viscosity as a function of the local shear rate. Using the plateau data and the shear-thinning trend line Fig. 8, the parameters m and n for the power-law model of the 61% volume fraction NNF in regimes R_3 and R_4 can be determined to be $m=7700$ Pa s, $n=1.0$ and $m=10,800$ Pa s, $n=0.19$, respectively.

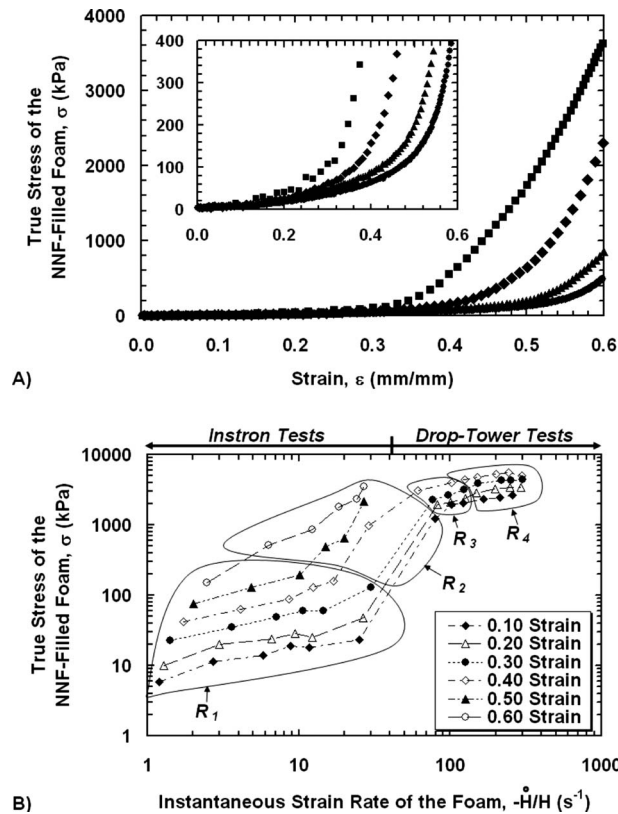


Fig. 9 (a) True stress plotted against strain for a 70 pores/in. foam filled with 61% volume fraction silica-based non-Newtonian fluid. $-\dot{H}=31.25$ mm/s (\bullet), 62.5 mm/s (\blacktriangle), 125 mm/s (\blacklozenge), and 250 mm/s (\blacksquare), corresponding to instantaneous strain rates of 2.5 s $^{-1}$, 5 s $^{-1}$, 10 s $^{-1}$, and 20 s $^{-1}$ at $\varepsilon=0.0$ strain, respectively. (b) True stress plotted against instantaneous strain rate for a 70 pores/in. foam filled with 61% volume fraction silica-based non-Newtonian fluid. Regimes R_1 – R_4 correspond to fluid behavior regimes.

5 Fluid-Filled Foam Results and Discussion

A plot of the true stress-strain responses of the 70 pores/in. foam saturated with the 61% volume fraction non-Newtonian fluid loaded at constant velocities ranging from 31.25 mm/s to 250 mm/s is given in Fig. 9(a). The dramatic increase in the true stress of the NNF-filled foam with strain is evident. The true stress of the NNF-filled foam is taken to be the load divided by current area, which is calculated based on conservation of mass, as previously discussed. At any given strain, the true stress of the NNF-filled foam and the corresponding instantaneous strain rate of the foam can be determined. The recorded data and Fig. 9(a) are used to generate the sample curve of the true stress response of the NNF-filled foam plotted against the instantaneous strain rate of the foam given in Fig. 9(b). For instantaneous strain rates less than 50 s $^{-1}$, strains varying from 0.1 to 0.6 are plotted in increments of 0.1, corresponding to aspect ratios ranging from approximately 1 to 4. For instantaneous strain rates greater than 50 s $^{-1}$ strains varying from 0.1 to 0.4 are plotted, corresponding to aspect ratios ranging from 1 to 2.

The dynamic compressive response of the saturated NNF-filled foam exhibits multiple regimes of behavior similar to the simple shear behavior of the fluid itself given by the previous rheological experiments (Figs. 7 and 8). As shown in Fig. 9(b), this behavior corresponds to the first four regimes (R_1 – R_4) of the fluid, previously discussed. At low instantaneous strain rates of the foam, the rate of increase in true stress of the NNF-filled foam with instantaneous strain rate is actually less than that of a comparable New-

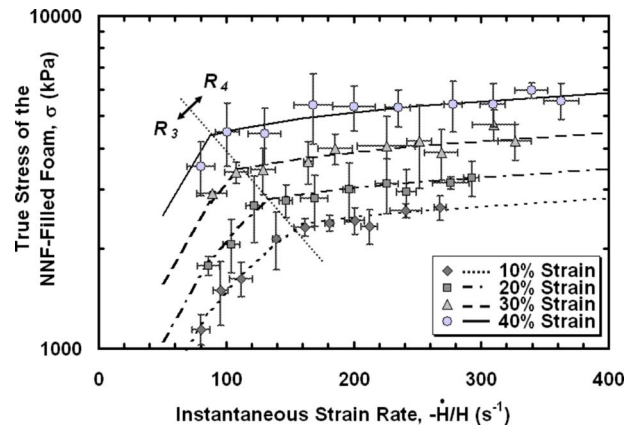


Fig. 10 True stress plotted against instantaneous strain rate for a 70 pores/in. foam filled with 61% volume fraction silica-based non-Newtonian fluid, ranging from 0.10 to 0.40 strain. The model corresponds to regimes R_3 and R_4 of the fluid given by Eq. (10).

tonian fluid, indicating the viscosity drops with increasing instantaneous strain rate, corresponding to the shear-thinning regime R_1 . The onset of the shear-thickening regime, corresponding to R_2 , is also evident and, as expected, is found to occur with increasing strain (or aspect ratio) or increasing instantaneous strain rate. Similarly, behaviors corresponding to regimes R_3 and R_4 are also evident. While distinguishing the transition between the upper plateau regime R_3 and the shear-thinning regime R_4 in Fig. 9(b) may be difficult at the given scale, the distinction is more apparent in expanded scales provided later in Fig. 10.

In this study, we are primarily interested in modeling the behavior after shear thickening has occurred (R_3 and R_4) since most engineering applications will utilize the NNF in this regime. For example, the expected impact velocities for a helmeted head in a motorcycle accident and a chest covered by standard body armor subjected to a 1 kg trinitrotoluene (TNT) blast wave at a distance of 1 m are on the order of 5 m/s and 10 m/s, respectively. This results in instantaneous strain rates for a 0.01 m thick foam sample of 500 s $^{-1}$ and 1000 s $^{-1}$, which are clearly beyond the instantaneous strain rate of the foam required for the fluid to transition from regime R_2 to regime R_3 (Fig. 9(b)). In addition, our focus was on modeling the behavior in regime R_3 and beyond because analytically modeling the behavior at strain rates less than those of regime R_3 is a complex task, which requires accounting for the fluid-structure interaction and the dramatic variation of the viscosity across the specimen. As previously discussed this problem is avoided for strain rates beyond the transition strain rate between regimes R_2 and R_3 , where the effects of the fluid-structure interaction and the foam itself can effectively be neglected.

To compare our model (Eq. (9)) with our data, in the upper plateau regime R_3 and in the shear-thinning regime R_4 , we examine data beyond the transition strain rate between regimes R_2 and R_3 . Figure 10 shows the true stress response of a 70 pores/in. foam filled with the non-Newtonian fluid under dynamic compression plotted against the instantaneous strain rate of the foam for a range of strains varying from $\varepsilon=0.10$ to $\varepsilon=0.40$ and a range of instantaneous strain rates ranging from ~ 50 s $^{-1}$ to ~ 400 s $^{-1}$. Each point is the average of four data points with error bars corresponding to one standard deviation. The error bars in the true stress direction are quite large as expected since small variations in the volume fraction of the silica particles in the fluid can result in large changes in viscosity but nearly no change in the exponent variable n . Correspondingly, the error bars in the instantaneous strain rate direction arise because changes in the energy absorption of the NNF-filled foam result in changes in the energy of

impacting drop tower and thus its velocity. The true stress contribution predicted by the model given by Eq. (9) is plotted in Fig. 10 for both the plateau regime R_3 and the shear-thinning regime R_4 , with their corresponding parameters m and n . To fit the true stress model constants C_{Ri} were introduced for each regime (where i corresponds to the regime) into Eq. (9) giving

$$\sigma_{\text{avg}} = 2C_{Ri} \left(\frac{2n+1}{n} \right)^n \frac{m}{n+3} \left(\frac{R_o}{H_o} \right)^{n+1} \left(\frac{-\dot{H}}{H} \right)^n \left(\frac{1}{1-\varepsilon} \right)^{3(n+1)/2} \quad (10)$$

The constants C_{R_3} and C_{R_4} given in Eq. (10) were found by establishing a measure of the goodness of fit and finding the value of C_{R_3} and C_{R_4} , which maximizes this measure. The measure for the goodness of fit R^2 is taken to be the sum of the squares of the difference between the experimental values and the average experimental value divided by the sum of the squares of the difference between the experimental values and the predicted values. Based on this measure of the goodness of fit, the empirical constants for regimes R_3 and R_4 are determined to be $C_{R_3}=0.94$ and $C_{R_4}=80$, respectively. These constants can be attributed primarily to two factors. First, as previously discussed, even small variations in the volume fraction of particles can result in large changes in the viscosity curves and thus the observed average true stress. Second, the increased tortuosity of the fluid path in the foam may also play a substantial role since the flow through the foam is not identically in shear flow.

Using the constants C_{R_3} and C_{R_4} , the transition between the plateau regime R_3 and the shear-thinning regime R_4 is found by setting Eq. (10), evaluated with constants (m and n) corresponding to the plateau regime, equal to Eq. (10), evaluated with constants (m and n) corresponding to the shear-thinning regime. The resulting equation governs the transition between R_3 and R_4 and is found to be

$$\left(\frac{-\dot{H}}{H} \right) = \left(\frac{C_{R_4}}{3C_{R_3}} \right)^{1.23} \left(\frac{H_o}{R_o} \right) (1-\varepsilon)^{3/2} \quad (11)$$

Using Eq. (11), for any given initial aspect ratio and strain, the instantaneous strain rate, corresponding to the transition between regimes R_3 and R_4 , can be determined. While Eq. (11) is not generalized for all fluids discussed in this paper, it is applicable to the 61% silica-based non-Newtonian fluid, which is the focus of this analysis. Since there is no model for the transition between the shear-thickening regime R_2 and the plateau regime R_3 , the onset of the behavior corresponding to R_3 is not predicted in this study; the model was plotted down to an arbitrary instantaneous transition strain rate of the foam selected to be 50 s^{-1} .

The constants C_{R_3} and C_{R_4} are found to be independent of the initial aspect ratio, the strain, and the instantaneous strain rate of the foam as demonstrated in Fig. 10. Furthermore, the constants C_{R_3} and C_{R_4} are also found to be independent of the grade of the foam beyond the shear-thickening transition. An additional study was performed to analyze the effects of varying the pore size of the foam. The true stress response of the NNF-filled foam was compared for 70 pores/in., 80 pores/in., and 90 pores/in. foam both prior to and after shear thickening (regimes R_2 and R_4). Prior to shear thickening, the true stress response is found to be highly dependent on the grade of the foam as demonstrated with Newtonian fluids [7]. Prior to shear thickening, the standard deviation in the true stress response of the three foam grades as a percentage of the average value was found to be 17.7%, which corresponds well with the results presented in Ref. [7]. However, after shear thickening has occurred, the true stress response of the NNF-filled foam is found to be independent of the grade of the foam, with a standard deviation in the true stress as a percentage of the average value of only 2.7%. This finding further supports the evidence shown in Fig. 2 that the fluid-structure interaction is negligible at

high loading rates (high stresses) after shear thickening has occurred. Thus, the constants C_{R_3} and C_{R_4} are independent of the grade of the foam beyond the shear-thickening transition.

The need for the introduction of the empirical constants C_{R_3} and C_{R_4} is expected and can primarily be attributed to the fact that small variations in the volume fraction of the silica particles in the fluid can result in large changes in viscosity, corresponding to m in Eq. (10), but nearly no change in the exponent variable n . This effect could readily account for such an apparently large constant while explaining the fact that the true stress scales accurately with all of the parameters in Eq. (10). The need for different empirical constants for each regime (C_{R_3} versus C_{R_4}) can also be seen through this argument. If the actual plateau viscosity is higher than that measured in the rheological experiments, the need for a constant greater than unity is evident for regime R_4 . Correspondingly, this effect would necessitate a constant greater than unity in regime R_3 as well; however, since regime R_3 only spans a very short range of local strain rates and local strain rates are expected to vary strongly over the radius of the foam, it is expected that not all of the fluid is accurately modeled by the maximum plateau viscosity (regime R_3). This would result in the model overestimating the average viscosity in the fluid and necessitating a constant less than unity to account for this overestimation. This effect would be less pronounced in the shear-thinning regime R_4 since the range of local strain rates spanned by this regime is much larger than that of R_3 . Therefore, the need for different constants for each regime (C_{R_3} versus C_{R_4}) is evident. The effects overall result in a constant for regime R_3 , which is on the order of unity, and a constant for regime R_4 , which is much greater than unity.

The empirical constants C_{R_3} and C_{R_4} may also indicate that a number of effects, which have been neglected based on the assumptions of the analysis, may be important. For instance, this analysis does not consider the tortuosity in the fluid path in the open-cell foam, which may also contribute to the need for the constants C_{R_3} and C_{R_4} , to be introduced. In addition, this model assumes that the radial velocity is uniform in the z -direction or that the fluid remains in a cylindrical shape as it undergoes deformation. This is a strong assumption as demonstrated in Fig. 1, where little variation in the radius up to 0.30 strain is detectable. However, even small variations in the radius of the NNF-filled foam can result in changes in the local shear rate profile, giving rise to large discrepancies between the predicted viscosity and the actual viscosity in the experiment and thus a discrepancy in the true stress response of the NNF-filled foam. Furthermore, this model uses the lubrication approximation, which assumes that the velocity in the z -direction is much less than the velocity in the r -direction, and the corresponding pressure drop in the z -direction is negligible compared with that in the r -direction. The lubrication approximation technique is known to be a powerful method for solving complex viscous flows. When applied to actual systems the fluid response is often found to converge very rapidly to the lubrication approximation as the ratio of the characteristic radius to the characteristic height is increased. Dawson et al. [7] found that the lubrication approximation for a Newtonian fluid-filled foam under dynamic compression is highly applicable beyond an aspect ratio of 4; however, examining their data shows that even for aspect ratios as small as 1 the lubrication model provides a good approximation. In the experiments presented in this paper the aspect ratios ranged from 1.17 to 3.95. Again, this could result in a small discrepancy in the local shear rate and a large discrepancy in the predicted true stress response of the NNF-filled foam from the model. Moreover, the fluid flow may not be considered entirely shear flow, which would result in a much lower predicted true stress response than actually observed experimentally. In addition, the local shear rate of the fluid may actually differ from that predicted by the model in part due to dependence on the fluid-foam interaction. Although this contribution is expected to be negligible the load response of the NNF-filled foam is three

orders of magnitude beyond that of the foam alone, and the characteristic diameter of the particles in the silica suspension is three orders of magnitude smaller than the characteristic pore size of the foam. Lastly, as previously discussed, this model assumes that the flow is dominated by viscous forces. This is an extremely robust assumption for the experiments presented in this analysis, considering the fluid viscosity increases approximately three orders of magnitude and approaches that of "solidlike" behavior after the shear-thickening transition. As previously discussed, the shear-thinning regime R_4 occurs over roughly four orders of magnitude of the local strain rate of the fluid, based on the behavior of fluid with lower volume fractions of particles, which have plateau regimes R_5 at a viscosity corresponding to the minimum viscosity of the fluid. Therefore, it is expected that the shear-thinning regime R_4 would also last several orders of magnitude of the instantaneous strain rate of the NNF-filled foam. Based on this, the fluid maintains an extremely high viscosity with increasing instantaneous strain rate for several orders of magnitude beyond the transition between the shear-thickening regime R_2 and the plateau regime R_3 . In the experiments presented in this paper, the maximum Reynolds was $Re=0.027$, which is much less than unity, demonstrating that the assumption that the flow is dominated by viscous forces is highly applicable. However, for extremely high rate loading scenarios, inertial forces may become more important and this viscous fluid assumption may no longer be valid. Therefore, this model may only provide an order of magnitude estimate beyond loading velocities of ~ 50 m/s (instantaneous strain rates of $\sim 5 \times 10^3$ s $^{-1}$) for samples with similar aspect ratios as those discussed in this paper. As previously discussed, nearly all comparable engineering designs used in dynamic compression, ranging from motorcycle helmets to blast loading protective equipment, would have loading rates applicable to this model.

Overall, the model for the true stress response of a non-Newtonian fluid-filled foam under dynamic compression given by Eq. (10) is strongly supported by experimental results, despite the need for a constant in each regime to account for some of the assumptions of the model. The model is found to describe the experimental results well for a variety of aspect ratios, strains, and instantaneous strain rates of the foam on the order of $-\dot{H}/H = 1.0 \times 10^2$ s $^{-1}$, independent of foam grade for a low-density elastomeric foam. The model is found to fall within one standard deviation of all of the experimental data presented in Fig. 10. A method is also presented to identify the transition instantaneous strain rate between regimes R_3 and R_4 , given an initial aspect ratio and strain.

6 Conclusion

A model for the true stress-strain response of a shear-thickening-fluid-filled, reticulated, elastomeric foam under dynamic compression beyond the shear-thickening transition is presented. This model is analytically tractable and useful in developing an understanding of the effects of material design parameters on the response of a NNF-filled foam under dynamic loading. To the authors' knowledge this is the first such analytical model, which explains this complex phenomenon for this selected group of non-Newtonian fluids and may be useful in the development of innovative new products in the field of protective equipment. In particular, this analytical model will be an essential step toward the successful development of a composite armor capable of impeding shockwaves caused by blast loading by providing insight into the energy absorption capabilities and wave propagation characteristics of a NNF-filled foam under dynamic loading.

Acknowledgment

This research was performed while on appointment as a National Defense Science and Engineering Graduate Fellow administered by the American Society for Engineering Education. This material is based on work supported by the National Science Foundation under Grant No. 0408259.

References

- [1] Cheeseman, B., and Bogetti, T., 2003, "Ballistic Impact Into Fabric and Compliant Composite Laminates," *Compos. Struct.*, **61**, pp. 161–173.
- [2] Bettin, G., and McKinley, G. H., 2005, "High Deformation Rate Behavior of Polymeric Foams Filled With Concentrated Silica Suspensions," Society of Rheology 77th Annual Meeting.
- [3] Hilyard, N. C., 1971, "Observations on the Impact Behaviour of Polyurethane Foams; II. The Effect of Fluid Flow," *J. Cell. Plast.*, **7**, pp. 84–90.
- [4] Rehkopf, J., Brodland, G., and McNeice, G., 1996, "Experimentally Separating Fluid and Matrix Contributions to Polymeric Foam Behavior," *Exp. Mech.*, **36**, pp. 1–6.
- [5] Mills, N., and Lyn, G., 2002, "Modeling Air Flow in Impacted Polyurethane Foam," *Cell. Polym.*, **21**, pp. 343–365.
- [6] Schraad, M., and Harlow, F., 2006, "A Multi-Field Approach to Modeling the Dynamic Response of Cellular Materials," *Int. J. Mech. Sci.*, **48**, pp. 85–106.
- [7] Dawson, M. A., McKinley, G. H., and Gibson, L. J., 2008, "The Dynamic Compressive Response of Open-Cell Foam Impregnated With a Newtonian Fluid," *ASME J. Appl. Mech.*, **75**(4), p. 041015.
- [8] Seguin, M. A., Montillet, A., Brunjail, D., and Comiti, J., 1996, "Liquid-Solid Mass Transfer in Packed Beds of Various Shaped Particles at Low Reynolds Numbers: Experiments and Model," *Chem. Eng. J.*, **63**, pp. 1–9.
- [9] Comiti, J. M., 1989, "A New Model for Determining Mean Structure Parameters of Fixed Beds From Pressure Drop Experiments: Application to Packed Beds With Parallelepipedal Particles," *Chem. Eng. Sci.*, **44**, pp. 1539–1545.
- [10] Sabiri, N. E., and Comiti, J. M., 1995, "Pressure Drop in Non-Newtonian Purely Viscous Fluid Flow Through Porous Media," *Chem. Eng. Sci.*, **50**, pp. 1193–1201.
- [11] Hoffman, R. L., 1974, "Discontinuous and Dilatant Viscosity Behavior in Concentrated Suspensions. II Theory and Experimental Tests," *J. Colloid Interface Sci.*, **46**, pp. 491–506.
- [12] Barnes, H. A., 1989, "Shear-Thickening ('Dilatancy') in Suspensions of Non-aggregating Solid Particles Dispersed in Newtonian Liquids," *J. Rheol.*, **33**, pp. 329–366.
- [13] Bossis, G., and Brady, J., 1989, "The Rheology of Brownian Suspensions," *J. Chem. Phys.*, **91**, pp. 1866–1874.
- [14] Farr, R. S., Melrose, J. R., and Ball, R. C., 1997, "Kinetic Theory of Jamming in Hardsphere Startup Flows," *Phys. Rev. E*, **55**, pp. 7203–7211.
- [15] Foss, D. R., and Brady, J. F., 2000, "Structure Diffusion and Rheology of Brownian Suspensions by Stokesian Dynamics Simulation," *J. Fluid Mech.*, **407**, pp. 167–200.
- [16] Catherall, A. A., Melrose, J. R., and Ball, R. C., 2000, "Shear Thickening and Order-Disorder Effects in Concentrated Colloids at High Shear Rates," *J. Rheol.*, **44**, pp. 1–25.
- [17] Bender, J., and Wagner, N., 1996, "Reversible Shear Thickening in Monodisperse and Bidisperse Colloidal Dispersions," *J. Rheol.*, **40**, pp. 899–916.
- [18] Maranzano, B. J., and Wagner, N. J., 2001, "The Effects of Particle Size on Reversible Shear Thickening of Concentrated Colloidal Dispersions," *J. Chem. Phys.*, **114**, pp. 10514–10527.
- [19] Maranzano, B. J., and Wagner, N. J., 2001, "The Effects of Interparticle Interactions and Particle Size on Reversible Shear Thickening: Hard-Sphere Colloidal Dispersions," *J. Rheol.*, **45**(5), pp. 1205–1222.
- [20] Bird, R. B., Armstrong, R., and Hassager, O., 1987, *Dynamics of Polymeric Liquids*, 2nd ed., Wiley, New York.
- [21] Yoshimura, A., and Prud'homme, R. K., 1988, "Wall Slip Corrections for Couette and Parallel Disk Viscometer," *J. Rheol.*, **32**(1), pp. 53–67.
- [22] Hager, S. L., and Craig, T. A., 1992, "Fatigue Testing of High Performance Flexible Polyurethane Foam," *J. Cell. Plast.*, **28**, pp. 284–303.
- [23] Lee, J. D., So, J. H., and Yang, S. M., 1999, "Rheological Behavior and Stability of Concentrated Silica Suspensions," *J. Rheol.*, **43**, pp. 1117–1124.
- [24] Hoffman, R. L., 1998, "Explanations for the Cause of Shear Thickening in Concentrated Colloidal Suspensions," *J. Rheol.*, **42**(1), pp. 111–123.
- [25] Laun, H. M., Bung, R., and Schmidt, F., 1991, "Rheology of Extremely Shear Thickening Polymer Dispersions," *J. Rheol.*, **35**, pp. 999–1034.
- [26] Hadjistamov, D., 1984, *Proceedings of the Ninth International Congress on Rheology*, M. B. Mena, R. Garca-Rejon, and C. Rangel, eds., Universidad Nacional Autonoma de Mexico, Acapulco, Mexico, p. 277.
- [27] Fagan, M., and Zukoski, C., 1997, "The Rheology of Charged Stabilized Silica Suspensions," *J. Rheol.*, **41**, pp. 373–397.
- [28] Egres, R., and Wagner, N., 2005, "The Rheology and Microstructure of Acicular Precipitated Calcium Carbonate Colloidal Suspensions Through the Shear Thickening Transition," *J. Rheol.*, **49**(3), pp. 719–746.